Journal of Applied Electrochemistry **33**: 393–401, 2003.

A study of copper deposition in the presence of Group-15 elements by cyclic voltammetry and Auger-electron spectroscopy

J. BRENT HISKEY[1] and Y. MAEDA[2]
[1]*Department of Materials Science and Engineering, University of Arizona, Tucson, AZ 85721, USA*
[2]*Hitachi Refinery, Nippon Mining and Metals Co., Ltd, Hitachi, Japan*

Received 3 March 2000; accepted in revised form 8 January 2002

Key words: cyclic voltammetry, deposition, spectroscopy

Abstract

The behaviour of arsenic, antimony, and bismuth during electrolytic refining of copper has been investigated using cyclic voltammetry, scanning electron microscopy, X-ray diffraction analysis and Auger electron spectroscopy. Electrodeposition was conducted using Group 15 element additions to two different cupric sulfate electrolytes: commercial tank house electrolytes containing 45 g l^{-1} Cu^{2+} and 200 g l^{-1} H_2SO_4 and liberator cell conditions containing 10 g l^{-1} Cu^{2+} and 400 g l^{-1} H_2SO_4. Analysis of electrochemical kinetic parameters indicates that the copper cathodes were more active at the higher sulfuric acid concentrations. SEM analysis revealed that Sb and Bi additions promoted truncated copper crystals while As-containing electrolytes produced random crystals. XRD patterns indicated Group 15 elements favour the production of (2 2 0) crystallographic orientation. Surface analyses of the copper deposits using AES techniques show that arsenic and antimony are deposited electrochemically forming primarily solid solution phases with copper in commercial tank house electrolytes. Under liberator cell conditions, a Cu_3As intermetallic phase forms when arsenic is present in the electrolyte. Antimony is present in solid solution under these conditions. Reduction of bismuth was not detected during these experiments.

1. Introduction

The amount of copper produced by hydrometallurgical techniques continues to increase due to improvements in solvent extraction and electrowinning (SX-EW) and the expansion of leaching activities. Electrowon cathode quality has improved dramatically in recent years and in some instances exceeds that of electrorefined copper. Despite the impressive advances in copper electrowinning, the majority of world copper is still produced from copper sulfide concentrates by pyrometallurigical and electrorefining techniques. However, the production of high quality electrorefined copper is increasingly more difficult because of the nature, concentrations, and variability of anode impurities.

Anode impurities that accumulate in the electrolyte can greatly influence the refining process. Group 15 elements (arsenic, antimony and bismuth) are especially important during the electrorefining of copper. The presence and behaviour of these contaminants can affect the cathode quality both in terms of being impurity constituents and by influencing the deposit structure and morphology. The incorporation of Group 15 elements in the cathode can occur by a number of possible mechanisms including: electrolytic codeposition; anode slime occlusion, electrolyte occlusion and direct precipitation of impurities from solution.

Schloen and Davenport [1] have reviewed operating data from 66 electrolytic copper refineries. The average concentration of arsenic, antimony and bismuth for the electrolyte in these plants was 6.20, 0.36 and 0.16 g l^{-1}, respectively. Arsenic is mainly present as the AsO_4^{3-} anion. It is the general view of operators that arsenic has no appreciable effect on electrolytic deposition of copper when the electrolyte does not contain antimony and bismuth. If antimony and bismuth are present in solution, then arsenic can form insoluble compounds with them under certain conditions. It is possible to form arsenate and antimonate precipitates with the general formula $(Sb,Bi,As)^{3+}(As,Sb)^{5+}O_4$. These compounds separate from the electrolyte as fine particles commonly referred to as 'floating slimes'. Braun et al. [2] and Abe [3] have attributed the presence of Group 15 impurities in copper cathodes to direct precipitation of arsenates onto the cathode surface and/or incorporation of 'floating slime' particles into the growing deposit.

Grigis and Ghali [4] conducted an electrochemical investigation to determine the behaviour of As(III) during electrodeposition of copper using a synthetic electrolyte containing 10.7 g l^{-1} Cu, 160 g l^{-1} H_2SO_4, and 2 g l^{-1} As maintained at 65 °C. They presented very useful information supporting the electrochemical deposition of arsenic at cathode potentials greater than −0.25 V. The reduction of arsenic was reported to occur

via As^{3+} and not As^{5+}. Surface analysis by XPS and AES techniques revealed the presence of As and As_2O_3. Sputtering appeared to remove the XPS peak belonging to As_2O_3 on deposits produced at −0.25 V. However, sputtering resulted in a XPS peak for As_2O_3 from an initial surface containing only As deposited at −0.58 V. This anomaly was attributed to the entrapment of layers of arsenic oxidized in the bulk electrolyte. It should be noted that the copper concentration in the synthetic electrolyte was relatively low (10.7 g l^{-1} Cu) compared to commercial operating conditions. In addition, the arsenic concentration of 2 g l^{-1} was also below the industrial average.

There remains considerable uncertainty about the exact mechanism of cathode contamination by Group 15 impurities. In copper electrorefining practice, the electrolyte system is very complex: there are many indifferent species; reactive inorganic and organic compounds; and certain decomposition products. The purpose of this study was to examine the electrochemical behavior of copper deposition in the presence of arsenic, antimony, and bismuth under controlled conditions. The electrochemistry of copper deposition from impurity-free and impurity-containing synthetic electrolytes was investigated using cyclic voltammetry (CV) methods. Deposit morphology and crystallographic orientation were examined by SEM and XRD techniques, respectively. Auger electron spectroscopy (AES) was used to examine the atomic composition of the copper deposit.

2. Experimental details

The electrochemical measurements were carried out using two different synthetic copper sulfate electrolytes. Electrolytes were prepared using AR grade or better chemicals and 18 MΩ water produced from a Milli-Q Plus and Milli-RO 10 Plus deionized water system. Type A electrolyte contained 45 g l^{-1} (0.71 M) Cu and 200 g l^{-1} (2.04 M) H_2SO_4. Group 15 element additions were made using As_2O_3 (5.0 g l^{-1} As), Sb_2O_3 (0.5 g l^{-1} Sb), and Bi_2O_3 (0.15 g l^{-1} Bi). Type C electrolyte contained 10 g l^{-1} (0.16 M) Cu and 400 g l^{-1} (4.08 M) H_2SO_4 and Group 15 elements equivalent to liberator cell conditions. The concentrations of As, Sb and Bi in type C electrolyte were 10, 1.0 and 1.0 g l^{-1}, respectively. Each electrolyte was deaerated by passing oxygen-free nitrogen through them for 1 h prior to the experiment. Type B electrolyte contained 10 g l^{-1} Cu and 200 g l^{-1} H_2SO_4 with additions of Group 15 elements at 1 g l^{-1} As, 0.5 g l^{-1} Sb and 0.15 g l^{-1} Bi. Type B electrolyte was used in linear sweep voltammetry reported elsewhere [5].

Cyclic voltammetry experiments were performed using type A and type C electrolytes at 63 °C in a 1 L conventional three-electrode cell. The electrochemical cell was submerged in a circulating water bath maintained at constant temperature, ±0.5 °C. High purity electrowon copper (~99.999%) was used for the working electrode and electrorefined copper (~99.99%) was used as a counter electrode. The working electrode (i.e., cathode) was machined into a disc and embedded into a PTFE rod with epoxy. The electrode area exposed to electrolyte during deposition was 0.48 cm^2. Prior to each test the working electrode was mechanically polished with different grades of silicon carbide paper and thoroughly rinsed with distilled, deionized water. The CV scans were performed successively and showed a high degree of reproducibility. A saturated calomel electrode (SCE) served as the reference electrode. The reference electrode was positioned within a Luggin capillary. The Luggin tip was placed close to the surface of the working electrode. This and the high-conductivity electrolyte effectively minimizes the IR error. At 63 °C, the SCE has a potential of 0.211 V vs the SHE (0.241 V at 25 °C).

A computer controlled EG&G PAR (model 273) potentiostat/galvanostat electrochemical measurement system was used throughout this investigation. Auger electron spectroscopy was performed using a Perkin Elmer (model PH1600) scanning Auger multiprobe. The SEM analysis was accomplished using a Joel JSM-840A scanning electron microscope. A Scintag XDS-2000 diffractometer was used to collect the XRD data.

3. Results and discussion

3.1. *Electrochemical behaviour*

The effect of Group 15 impurities on the basic electrochemical response of copper deposition was investigated using cyclic voltammetry. It is recognized that there exists some fundamental problems associated with CV for concentrated electrolytes similar to those in the case of interest. The analysis and interpretation of the voltammograms is difficult, but there is important information that can be derived from this type of study. Cyclic voltammograms ranging from +0.20 mV to −0.70 V vs SCE obtained as a function of scan rate (v) are shown in Figures 1 and 2 for the typeA electrolyte.

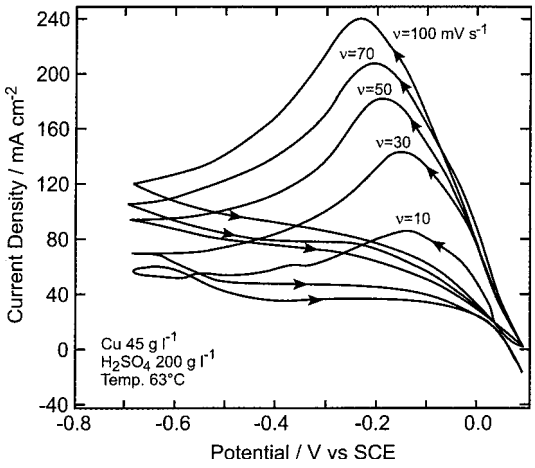

Fig. 1. Cyclic voltammograms of copper deposition in impurity free type A electrolyte as a function of scan rate.

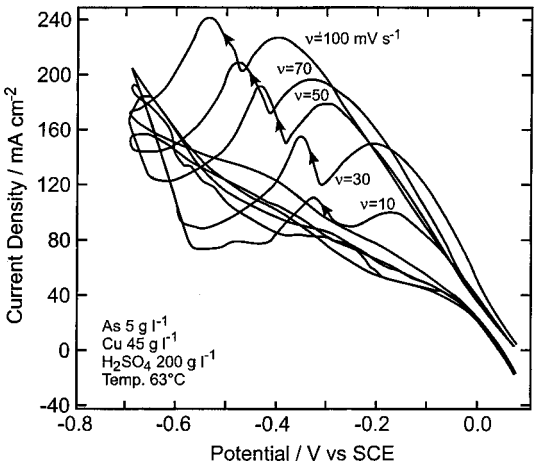

Fig. 2. Cyclic voltammograms for copper deposition in As-containing type A electrolyte as a function of scan rate.

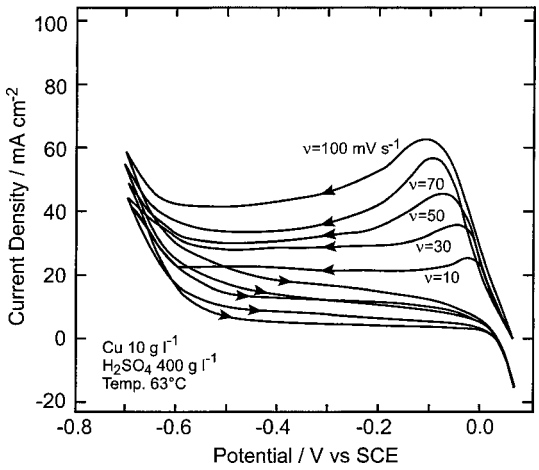

Fig. 3. Cyclic voltammograms for copper deposition in impurity free type C electrolyte as a function of scan rate.

The main wave in Figure 1 corresponds to the reduction of copper. The absence of an anodic peak upon the reverse scans suggests an irreversible charge transfer reaction. The shift in cathodic peak potential with increasing scan rate indicates a possible IR distortion in the CV data associated with the high current density values. The voltammograms shown in Figure 2 for the 5 g l^{-1}. As system reveal the main peak for copper reduction and a well defined second reduction peak. The reaction associated with this wave is also irreversible. An order of magnitude increase in scan rate (v = 10 to 100 mV s^{-1}) results in a cathodic peak potential shift from −0.33 to −0.54 V vs SCE for the second peak. The peak potential shift for the second wave was associated with the IR distortion caused by the first wave. The potential shift (from the foot of the wave to the peak potential) for the second wave was about 50 mV for each scan. Scans for Sb and Bi containing type A electrolyte appeared very similar to the impurity-free electrolyte. Strong peaks corresponding to the reduction of either antimony or bismuth were not detected using the type A electrolyte composition. The slowest scan (v = 10 mV s^{-1}) for antimony, however, does exhibit two minor shoulders on the main wave.

Type-C electrolyte compositions, typical of liberator cell conditions, were used to obtain the CV scans in Figures 3–5. The reasons for using liberator cell conditions were: (i) elimination of surface passivation (i.e., $CuO + 2\,H^+ = Cu^{2+} + H_2O$), and (ii) investigation of the electrochemical behavior at higher antimony and bismuth concentrations. The electrochemical response under these conditions is clearly different than that obtained with type-A electrolytes. As shown in Figure 3, the peak current density associated with the reduction of copper is lower by about a factor of 4, and again, the shift in peak potential is affiliated with the IR distortion. There are three peaks in the scan for the As-containing type C electrolyte, and two peaks in the Sb-containing electrolyte, as revealed in Figures 4 and 5, respectively. Scans for the Bi-containing type C electrolyte appeared very similar to impurity free electrolyte, however, the

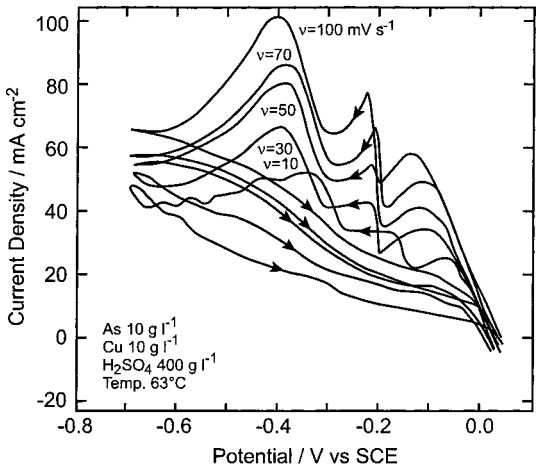

Fig. 4. Cyclic voltammograms for copper deposition in As-containing type C electrolyte as a function of scan rate.

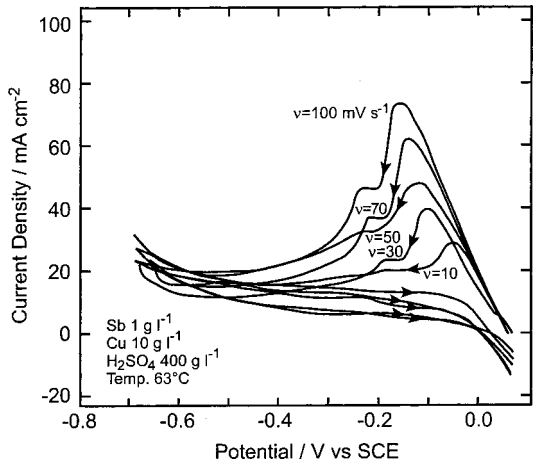

Fig. 5. Cyclic voltammograms for copper deposition in Sb-containing type C electrolyte as a function of scan rate.

slowest scan (v = 10 mV s^{-1}) exhibited minor shoulders on the cathodic side of the main wave. Higher concentrations of Group 15 elements and a more active

Table 1. Equilibrium and standard reduction potentials for type A electrolyte conditions

	Reaction	E° /V		E_{eq} /V		E_{eq} /V
		25 °C	63 °C	25 °C	63 °C	63 °C
1	$Cu^{2+} + 2\,e^- = Cu$	0.339	0.340	0.254	0.260	0.049
2	$HAsO_2 + 3\,H^+ + 3\,e^- = As + 2\,H_2O$	0.247	0.229	0.218	0.193	−0.018
3	$SbO^+ + 2\,H^+ + 3\,e^- = Sb + 2\,H_2O$	0.293	0.282	0.242	0.222	0.011
4	$Bi^{3+} + 3\,e^- = Bi$	0.143	0.126	0.077	0.052	−0.159
5	$H_3AsO_4 + 2\,H^+ + 2\,e^- = HAsO_2 + 2\,H_2O$	0.576	0.568	0.575	0.524	0.313
6	$H_3AsO_4 + 4\,H^+ + 4\,e^- = As_2O_3 + 5\,H_2O$	0.597	0.583	0.554	0.530	0.319
7	$3\,Cu^{2+} + HAsO_2 + 3\,H^+ + 9\,e^- = Cu_3As + 2\,H_2O$	0.323	0.317	0.257	0.252	0.041

electrode surface (high H_2SO_4 concentration) result in more detail in the CV patterns.

The equilibrium reduction potentials (E_{eq}) for copper and the reactions involving Group 15 elements at 25 and 63 °C have been determined using the Nernst equation. Standard reduction potentials (E°) were calculated with the aid of the HSC Chemical Reaction and Equilibrium Software distributed by Outokumpu Research Oy, Pori, Finland. Table 1 shows the results of these evaluations.

Estimates for solution speciation and individual activity coefficients for the type A electrolyte were obtained from Zheng [6]. The equilibrium reaction potentials for the various reactions against the standard calomel electrode (0.211 V at 63 °C) are listed in the right hand column of Table 1.

The reduction of antimony and bismuth was not detected in type A electrolytes. Antimony has an E_{eq} (63 °C) value of about 38 mV below that for Cu and its reduction peak is likely hidden by that for copper. Furthermore, the concentrations of antimony and bismuth are low and therefore fail to produce a detectable CV signature. As shown in Figure 2, the presence of arsenic at 5 g l^{-1} shows a second reduction wave. Based on the information in Table 1, this is likely attributed to Reaction 2.

In As-containing typeC electrolyte, three reduction peaks were observed. The sharp peak at about (2nd reduction peak) −0.200 V vs SCE possibly related to the formation of Cu_3As as an intermetallic phase according to Reaction 7.

3.2. *Analysis of cathodic current maxima*

Schab and Hein [7] have addressed the problems associated with cathodic mass transfer in copper refining electrolyte at increased current density. They concluded that migration contributions can be neglected because of the small transport number ($t_{cu^{2+}} = 0.02$) for cupric ions. Furthermore, under the conditions of these experiments natural convective forces near the electrode will not develop within the short transition times. Therefore, within the framework of this investigation, mass transfer by diffusion would dominate.

Peak current response of irreversible electrode processes has been analyzed by Berzins and Delahay [8]. Andricacos and Ross [9–11] have furnished detailed analysis of metal deposition at stationary and rotating-disk electrodes. For multisweep cyclic voltammetry, the cathodic current maximum is described by the following relationship:

$$i^l_{c,max} = \frac{n^{3/2}F^{3/2}}{R^{1/2}T^{1/2}} D^{1/2} C_b v^{1/2} I^l_{c,max}[(at_c)^l_{max}; a\theta] \qquad (1)$$

where l is the number of complete sweeps, D the diffusion coefficient, C_b the bulk concentration, v the sweep rate, $I^l_{c.max}[(at_c)^l_{max}; a\theta]$ a cathodic current density function, and (n F R T) have their usual meanings. Derivation of the current density function was provided in the Appendix of [10] for deposition on a stationary planar electrode. For a single sweep CV, the current density function is defined by the following equations:

$$I^l_c(at_c) = 2\pi^{-1/2} f[(at_c)^{1/2}] \qquad (2)$$

$$f(x) = \exp(-x^2) \int_0^x \exp(u^2)\mathrm{d}u \qquad (3)$$

where the term a is defined as $(nF/RT)v$, t_c is the time into the cathodic sweep, and θ is the duration of the cathodic part of the CV sweep. The values of $i^\circ_{c,max}$ for the main copper deposition wave for type A and type C electrolytes were taken from the respective CV plots. The values of the current density function ($I^\circ_{c,max}$) were calculated using Equations 2 and 3 and taking t_c as the time into the sweep to reach the position of the cathodic maximum.

Plots of $i^\circ_{c,max}/I^\circ_{c,max}$ vs $v^{1/2}$ are shown in Figure 6 for copper deposition in both impurity free type A and type C electrolytes. The experimental data for the main copper deposition wave corresponds very well with the predictions made in Equation 1. The value of $D_{Cu^{2+}}$ can be calculated from the slopes of these lines for the two different electrolytes. The slopes yield $D_{Cu^{2+}}$ values of 2.9×10^{-5} and 1.9×10^{-5} cm^2 s^{-1} for type A and type C electrolyte, respectively. These values are compared in Table 2 for electrolyte type A and C containing As, Sb, and Bi, respectively. They are higher than those found using other techniques. At 63 °C in an impurity free electrolyte containing 45 g l^{-1} Cu^{2+} and 200 g l^{-1} H_2SO_4 a diffusion coefficient for copper of

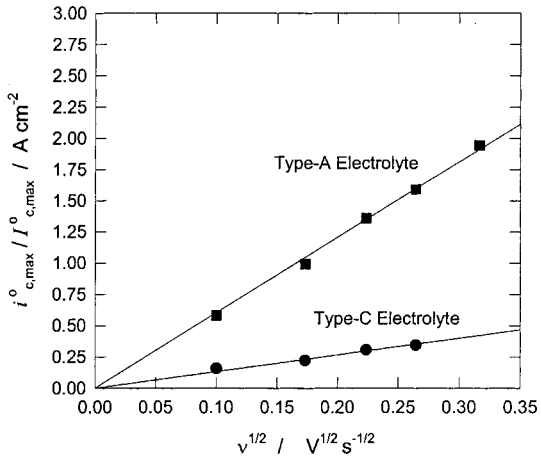

Fig. 6. Dependence of the maximum cathodic current on the square root of the sweep rate for the main copper deposition peak in impurity free type A and type C electrolytes.

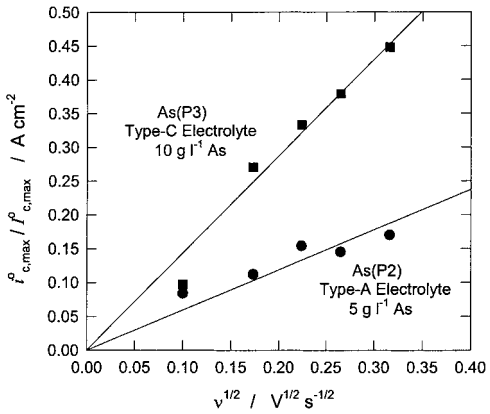

Fig. 7. Dependence of the maximum cathodic current on the square root of the sweep rate for As(P2) wave in impurity free type A and type C electrolytes.

1.0×10^{-5} cm^2 s^{-1} was calculated from rotating disc electrode (RDE) limiting current measurements [12] and density and viscosity data published by Price and Davenport [13]. The marked discrepancy in diffusivity values is believed to be associated with the estimation of the value of t_c. For example, at the fastest scan rate a difference of only a few seconds in t_c can account for the difference in $D_{Cu^{2+}}$. At 63 °C in an impurity free electrolyte containing 10 g l^{-1} Cu^{2+} and 200 g l^{-1} H_2SO_4, a diffusion coefficient value for copper of 1.3×10^{-5} cm^2 s^{-1} was calculated from rotating-disc electrode (RDE) limiting current measurements [12] and using density and viscosity data published by Price and Davenport [13].

Based on the analysis of $i^{\circ}_{c,max}/I^{\circ}_{c,max}$ vs $v^{1/2}$, the presence of Group l5 impurities have little if any effect on current density maxima for the copper deposition peak for both type A and type C electrolytes.

The second peak in the As-containing type A electrolyte represents the irreversible reduction of arsenic from the trivalent state according to Reaction 2. Slope analysis for the $i^{\circ}_{c,max}/I^{\circ}_{c,max}$ vs $v^{1/2}$ data for the second peak is shown in Figure 7. The rise time (t_c) for the second cathodic peak was measured from the foot of the As (P2) wave. The experimental data for the second wave in the As-containing electrolytes agrees very well with the predictions made in Equation 1. Data for the deposition at As (P2) suggest a diffusion coefficient for the arsenic species of about 0.9×10^{-5} cm^2 s^{-1} in type A electrolyte. In the type C electrolyte that contains 400 g l^{-1} H_2SO_4 the diffusivity of arsenic was determined to be 1.3×10^{-5} cm^2 s^{-1}. Analysis of current maximum data for the As (P3) wave in the type C electrolyte indicates nearly identical behaviour to that for As (P2) in type A.

3.3. *Morphological studies*

Morphological studies using scanning electron microscopy [14] indicated that the copper deposit was clearly characterized by random crystal growth for the impurity-free electrolyte at a current density of 250 A m^{-2}. At 500 A m^{-2} the tendency in the impurity-free electrolyte was more towards a dendritic structure. This comparison is shown in Figure 8(a) and (b). The deposit morphology for the arsenic containing electrolyte was similar to that for the low current density impurity-free electrolyte for both 250 and 500 A m^{-2}. As revealed in Figure 9(a) and (b), antimony and bismuth appeared to promote truncated copper crystals, Figure 10 reveals a fault star and associated crystal twinning found with the deposition of copper from Sb-containing type A electrolyte. This indicates the presence of considerable dislocations in the electrodeposited copper for antimony and bismuth containing electrolyte. Twinning in the fault star is probably the (1 1 1) direction according to Ogburn and Newton [15].

The crystallographic orientation of copper deposited on test cathodes was examined using XRD techniques [14] and the results are summarized in Table 3. The substrate had a (1 1 1) texture and deposition from the impurity-free electrolyte essentially retained this

Table 2. Diffusion coefficients for copper in type A and C electrolytes

Diffusion coefficients (63 °C)/cm^2 s^{-1}							
Type A electrolyte				Type C electrolyte			
Impurity free	As 5 g l^{-1}	Sb 0.5 g l^{-1}	Bi 0.15 g l^{-1}	Impurity free	As 10 g l^{-1}	Sb 1 g l^{-1}	Bi 1 g l^{-1}
2.9×10^{-5}	3.8×10^{-5}	3.3×10^{-5}	3.5×10^{-5}	1.9×10^{-5}	1.6×10^{-5}	3.4×10^{-5}	2.5×10^{-5}

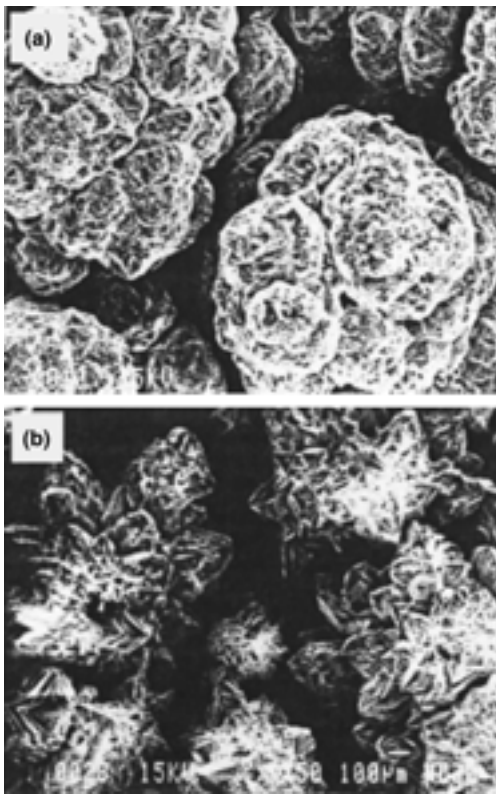

Fig. 8. Copper deposit from impurity-free type A electrolyte, position B for current densities of (a) 250 A m^{-2} and (b) 500 A m^{-2}.

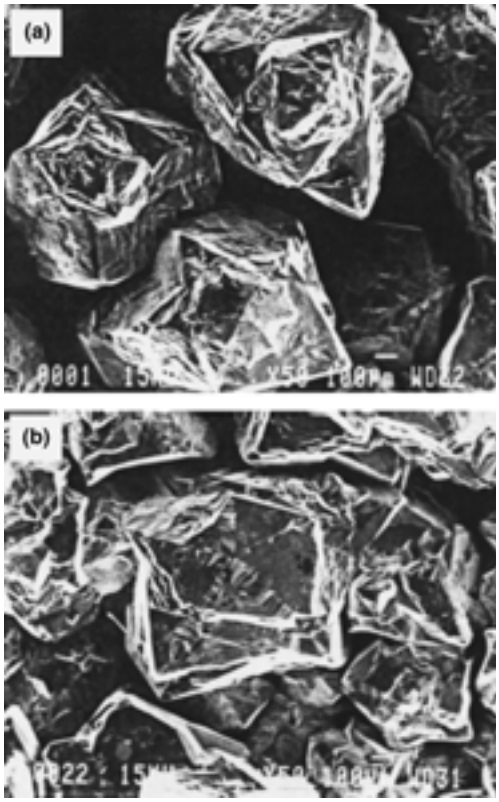

Fig. 9. Copper deposit at 250 A m^{-2}, position B for (a) Sb-containing and (b) Bi-containing type A electrolyte.

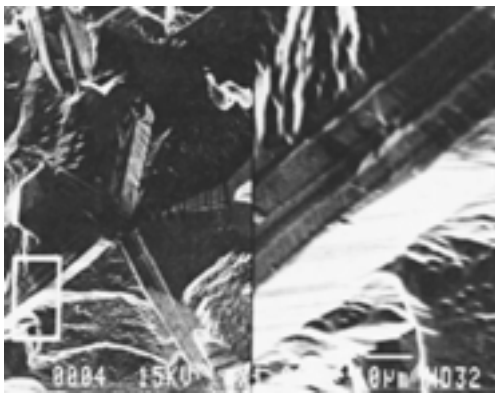

Fig. 10. A fault star and the associated twinning in the copper deposit from Sb-containing type A electrolyte at 250 A m^{-2}.

Table 3. X-Ray diffraction orientation data for copper deposits from type A electrolyte

Electrolyte	Position	Intensity ratio		
		(1 1 1)	(2 0 0)	(2 2 0)
Impurity-free	A	100	46	27
	B	100	77	58
	C	54	26	100
As-containing	A	89	51	100
	B	87	82	100
	C	64	32	100
Sb-containing	A	25	39	100
	B	0	20	100
	C	16	19	100
Bi-containing	A	0	0	100
	B	0	0	100
	C	0	0	100
Substrate (starter sheet)		100	46	43

Identification of cathode sampling position 

orientation. However, analysis of the XRD patterns showed that the addition of Group 15 tended to favour the (2 2 0) orientation. These findings support the results of O'Keefe et al. [16] which showed that under tank house conditions that there was a tendency toward (2 2 0) orientation with increasing Sb concentration. Deposit orientation and crystal faceting during copper deposition have been the subject of a number of investigations [17–20]. de Cusminsky [21] characterized the stages of deposition as (a) epitaxial growth, (b) twin development and (c) polycrystalline growth. The deposit thickness just prior to polycrystalline deposition follows the order:

$$h_{o(111)} < h_{o(100)} < h_{o(110)}$$

Atomic density for the crystal planes follows this same order. Bockris and Kita [17] suggested that the (1 1 1) facet grows faster than the (1 0 0), and thus eliminate themselves and increasing the proportion of 1 0 0 planes on the surface.

3.4. *Auger studies*

Auger electron spectroscopy (AES) was used to analyse surface deposits produced at conditions corresponding to the various peaks observed in the CV measurements. Chronoamperometry experiments were performed to determine transient time constants and to provide samples for AES analysis. Arsenic transient times were observed to be about 30 s for both type A and type C electrolytes [14]. Furthermore, there was very little difference between the As-containing electrolyte and the impurity-free electrolyte after 9 s. A deposition time of 30 s was selected for the As-containing electrolyte.

3.4.1. *Type A electrolyte*

Auger electron spectra for electrodeposition in a potential region (−0.330 V vs SCE) of the second peak in As-containing type A electrolyte is shown in Figure 11(a) and (b) before and after sputtering, respectively. The spectra indicate peaks due to arsenic at 1224 eV and 1263 eV for this electrolyte. After sputtering, the peaks for carbon and oxygen decrease significantly; however, by comparison, those for arsenic do not change substantially. This indicates that arsenic deposits electrochemically. If elemental arsenic is the product as suggested by Reaction 2 in Table 1, then reduction is from the As^{3+} oxidation state. It is noticed that the oxygen peak at 513 eV persists in the sputtered sample. As_2O_3, which is thermodynamically possible, could be a stable product as predicted by Reaction 6. XPS and AES studies by Girgis and Ghali [4] found that reduction of arsenic proceeds through As^{3+} to form either metallic As or As_2O_3. However, based on the CV pattern for As-containing type A electrolyte and the relative E_{eq} values for Reactions 2 and 6 it is believed that reduction at As (P2) is predominantly to elemental As. There is a likelihood that As_2O_3(c) could form according to

$$2HAsO_2 = As_2O_3(c) + H_2O$$

$$K_{63} = 6.12$$

and be entrapped in the electrode surface. However, at 63 °C, the activity of $HAsO_2$ would have to exceed 0.41 M for As_2O_3(c) formation. The activity of dissolved arsenic species is considerably below this value in type A electrolyte.

A peak for chlorine was observed at 181 eV for the type A electrolyte sample prior to sputtering. Chloride, along with other addition agents, is commonly used in modern copper electrorefining electrolytes at concentrations between about 20 and 40 ppm. Yao [16] reports that chloride ions function as follows: (i) chemically it precipitates silver as silver chloride, and antimony and bismuth as oxychlorides; (ii) electrochemically it acts as a cathode depolarizer; and (iii) physically it serves as a grain refiner. Chloride in the test electrolyte comes from the copper sulfate reagent used to prepare the electrolyte and has been found to be < 3 ppm. Chloride is removed after sputtering as shown in Figure 11(b).

AES analysis of deposits obtained at the main deposition wave did not detect the presence of Sb and Bi from the type A electrolytes.

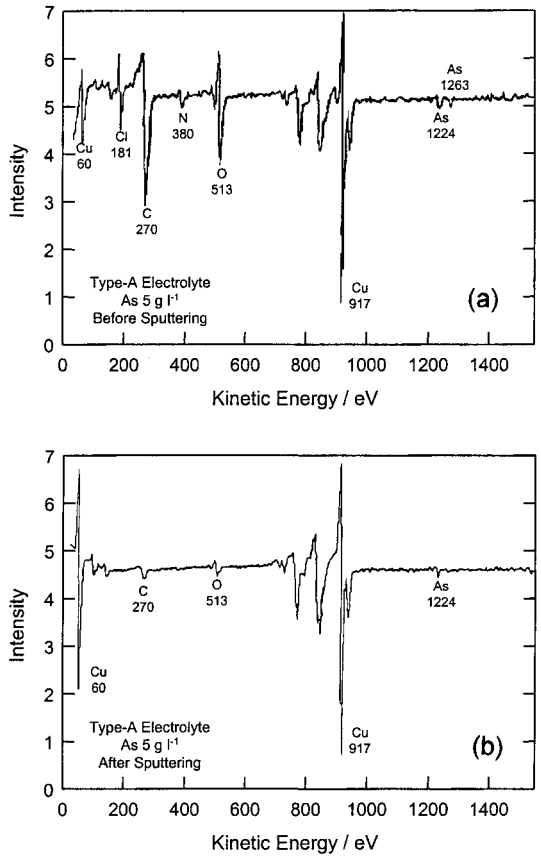

Fig. 11. Auger electron spectra of electrodeposition at the 2nd peak in the type A electrolyte containing As. (a) Before sputtering and (b) after sputtering.

3.4.2. *Type C electrolyte*

The AES analyses were performed on deposits from As containing type C electrolyte at the second peak (P2). Arsenic peaks in the AES spectrum for the after sputtering specimen are shown in Figure 12(a). Peaks at 1030, 1127, 1224 and 1263 eV were observed in the sample before and after sputtering. Sputtering removed most of the carbon and oxygen, while the arsenic remained essentially unchanged. These were the most intense As peaks detected by Auger in this study, suggesting that an arsenic rich phase is being deposited at −0.200 V vs SCE. It is known that the black porous deposits on liberator tank house cathodes is copper arsenide produced according to Reaction 7. This is not surprising since the equilibrium electrode potential for the main copper deposition reaction and the reaction for the deposition of Cu_3As are nearly identical (0.049 V vs 0.041 V).

AES results for a deposit obtained for As-containing type C electrolyte at −0.383 V (P3) are shown in Figure 12(b) for the after sputtering sample. Clearly this specimen contained a large amount of oxygen.

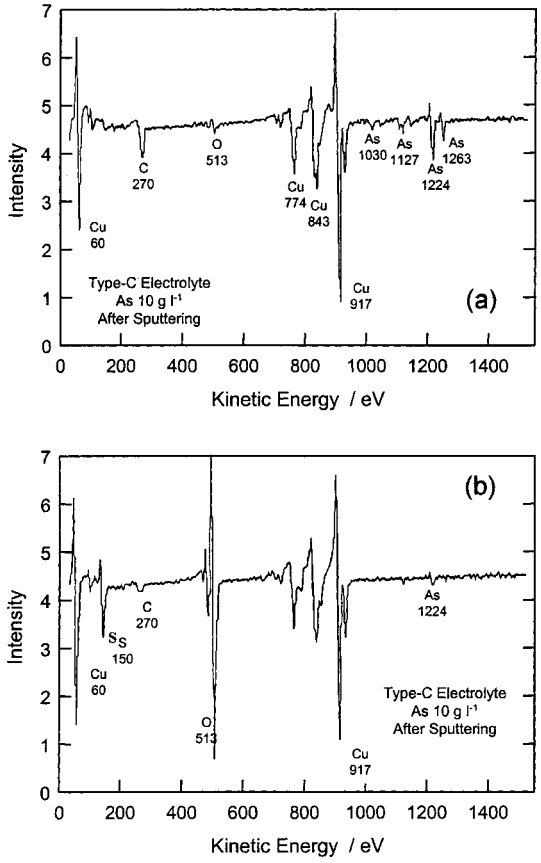

Fig. 12. Auger electron spectra after sputtering for electrodeposition in the type C electrolyte containing As. (a) Peak As(P2) and (b) peak As(P3).

Peaks for arsenic were absent in the before sputtering spectrum; however, arsenic peaks did appear after sputtering. The one at 1224 eV is labeled for reference. The oxygen signal remained quite intense even after sputtering; however, carbon was nearly removed by sputtering. Visual inspection of the electrode indicated an extremely rough and very porous surface. A possible reason for the large oxygen peaks is surface oxidation after electrodeposition. Alternately, the porous nature of the deposit may cause entrainment of electrolyte which results in the strong O and S peaks observed prior to and after sputtering. The intensity ratios for these peaks were O:S = 4.8 and 3.7 for before and after sputtering, respectively. The sputtered sample approaches a O:S ratio close to that for sulfate.

A sample produced in Sb-containing type C electrolyte at −0.193 V revealed Auger peaks for Sb at 384 and 453 eV. These peaks were present in spectra both generated before and after sputtering. The carbon and oxygen peaks were nearly completely removed in the after sputtering spectra. Therefore, the 2nd peak in the Sb system results from the simple reduction of antimony according to Reaction 3 shown in Table 1.

There were no AES peaks observed for the Bi system. This suggests that bismuth is not deposited electrochemically under the conditions of these experiments. This observation is confirmed by the absence of a deposition peak in the CV patterns for Bi-containing electrolytes, both type A and type C. The results of the AES analysis after sputtering are summarized in Table 4. Sputtering was performed in such a manner as to remove as much of the C as possible or to a point where the C reached a constant level. The concentration reported in Table 4 were determined by measuring peak to peak values and then applying a sensitivity factor. The composition reported is only a semiquantitative measure. Main peak analysis of the Auger spectra for surfaces after sputtering indicates a substantial increase in arsenic content for the 2nd peak from type A to type C electrolytes. This is consistent with the electrolyte composition and the increased surface activity with the type C electrolyte. Arsenic appears to be in solid solution for deposits formed from type A electrolytes. It is clear that a Cu_3As intermetallic phase is deposited under (P2) conditions from type C electrolytes.

Table 4. Summary of Auger electron spectra analysis for after sputtering

Electrolyte	Peak designation	Peak potential /mV	Composition /at %
As type A	2nd	−0.330	As 4.4 Cu 96.8
As type C	2nd	−0.200	As 23.5 Cu 76.4
	3rd	−0.383	As 3.0 Cu 58.6 O 38.2
Sb type C	2nd	−0.193	Sb 3.1 Cu 96.8
Bi type C	1st	−0.050	Bi ND

4. Conclusions

Copper deposition from electrolytes containing Group 15 impurities has been investigated using electrochemical, SEM and XRD techniques, and Auger electron spectroscopy (AES) studies. Simulated commercial tank house electrolytes (type A) containing arsenic revealed two reduction peaks. The first peak represents copper reduction and the second peak is associated with arsenic reduction from the As^{3+} oxidation state. AES analysis of the second peak shows that arsenic is predominantly deposited electrochemically according to the following possible reactions:

$$HAsO_2 + 3\,H^+ + 3\,e^- = As + 2\,H_2O$$

Type A electrolyte containing Sb and Bi exhibited electrochemical responses nearly identical to that for the impurity-free electrolyte.

Simulated liberator cell (type C) conditions revealed three reduction peaks for As-containing electrolyte, two peaks for Sb-containing electrolyte, and one for the Bi-containing electrolyte. In each case, the first wave

represents the reduction of copper. The second peak for the arsenic system appears to be associated with the formation of the Cu_3As intermetallic phase. However, the third peak reveals the formation of considerable surface oxidation. The second peak in the Sb-containing electrolyte corresponds to the reduction of antimony according to Reaction 3:

$$SbO^+ + 2\,H^+ + 3\,e^- = Sb + H_2O$$

Reduction of bismuth was not detected. The peak for bismuth reduction was likely concealed by that for copper. In general, copper cathodic surfaces appear more active under type C electrolyte conditions. AES results support the electrochemical observations related to Group 15 elements. However, there remains some uncertainty regarding the formation of As_2O_3 as a secondary phase from solution.

SEM analysis showed that Sb and Bi additions promote truncated copper crystals as compared to random crystals in the impurity-free and As-containing electrolytes. X-ray diffraction pattern analysis revealed that addition of Group 15 elements promoted the (2 2 0) compared with the impurity-free case that (1 1 1) crystallographic orientation of the substrate.

References

1. W.G. Davenport et al. 'Electrorefining and hydrometallurgy of copper', *in* Proceedings of the Copper 99 – Cobre 99 Fourth International Conference, J.E. Butrizac et al. (Eds), TMS, Warendale, PA (1999), pp. 3–93.
2. T.B. Braun, J.R. Rawling and K.J. Richards, *in* J.C. Yannopoulos and J.C. Agarwal (Eds), 'Extractive Metallurgy of Copper', AIME, New York (1976), pp. 511–524.
3. S. Abe, 'Research of Anode Passivation in Copper Refining', PhD thesis, University of Tokyo (1981).
4. M. Girgis and E. Ghali, *in* J.E. Hoffmann et al. (Eds), The Electrorefining and winning of Copper, TMS-AIME, Warrendale, PA (1987), pp. 173–193.
5. J.B. Hiskey and Y. Maeda, *in* R. Woods and P.E. Richardson (Eds), 'Proceedings of the Third International Symposium on Electrochemistry in Mineral and Metal Processing III', The Electrochemical Society, Pennington, NJ (1992), pp. 528–545.
6. Z. Zheng, 'Fundamental Studies of the Anode Behavior of Thiourea in Copper Electrorefining', PhD thesis, University of British Columbia (2000).
7. D. Schab and K. Hein, *Canadian Metall. Q.* **31** (1992) 173.
8. T. Berzins and P. Delahay, *J. Am. Chem. Soc.* **75** (1953) 555.
9. P.C. Andricacos and P.N. Ross, Jr., *J. Electrochem. Soc.* **130**(6) (1983) 1340.
10. P.C. Andricacos and P.N. Ross, Jr., *J. Electrochem. Soc.* **130**(6) (1983) 1340.
11. P.C. Andricacos and P.N. Ross, Jr., *J. Electrochem. Soc.* **131**(7) (1984) 1531.
12. M.S. Moats, J.B. Hiskey and D.W. Collins, *Hydrometallurgy* **52** (2000) 255.
13. D.C. Price and W.G. Davenport, *Met. Trans. B* **11B** (1980) 159.
14. Y. Maeda, 'The Behavior of Impurities During Copper Electrodeposition', MS thesis, University of Arizona (1991).
15. F. Ogburn and C. Newton, *J. Electrochem. Soc.* **110**(11) (1963) 1148.
16. T.J. O'Keefe and L.R. Hurst, *J. Appl. Electrochem.* **8** (1978) 109.
17. J. O'M. Bockris and H. Kita, *J. Electrochem. Soc.* **109**(10) (1962) 928.
18. U. Bertocci, *J. Electrochem. Soc.* **113**(6) (1966) 604.
19. U. Bertocci and C. Bertocci, *J. Electrochem. Soc.* **118**(8) (1971) 1287.
20. W.A. Schultze, *J. Crystal Growth* **13/14** (1972) 421.
21. J.B. deCusminsky, *Electrochim. Acta* **15** (1970) 73.
22. Y. Yao, *Trans. Electrochem. Soc.* **86** (1944) 371.